Acta Crystallographica Section D
Biological Crystallography
ISSN 1399-0047

3′-Azidothymidine in the active site of *Escherichia coli* thymidine phosphorylase: the peculiarity of the binding on the basis of X-ray study

Vladimir Timofeev,[a]* Yulia Abramchik,[a,b] Nadezda Zhukhlistova,[a] Tatiana Muravieva,[b] Ilya Fateev,[b] Roman Esipov[b] and Inna Kuranova[a]

[a]X-ray Analysis Methods and Synchrotron Radiation, Shubnikov Institute of Crystallography, Russian Academy of Sciences, Leninsky Prospect 59, Moscow, 119333, Russian Federation, and [b]Laboratory of Biotechnology, Shemyakin–Ovchinnikov Institute of Bioorganic Chemistry, Russian Academy of Sciences, Ul. Miklukho-Maklaya 16/10, Moscow, 117997, Russian Federation

Correspondence e-mail: tostars@mail.ru

Received 20 December 2013
Accepted 27 January 2014

PDB reference: thymidine phosphorylase, complex with AZT, 4lhm

The structural study of complexes of thymidine phosphorylase (TP) with nucleoside analogues which inhibit its activity is of special interest because many of these compounds are used as chemotherapeutic agents. Determination of kinetic parameters showed that 3′-azido-3′-deoxythymidine (3′-azidothymidine; AZT), which is widely used for the treatment of human immunodeficiency virus, is a reversible noncompetitive inhibitor of *Escherichia coli* thymidine phosphorylase (TP). The three-dimensional structure of *E. coli* TP complexed with AZT was solved by the molecular-replacement method and was refined at 1.52 Å resolution. Crystals for X-ray study were grown in microgravity by the counter-diffusion technique from a solution of the protein in phosphate buffer with ammonium sulfate as a precipitant. The AZT molecule was located with full occupancy in the electron-density maps in the nucleoside-binding pocket of TP, whereas the phosphate-binding pocket of the enzyme was occupied by phosphate (or sulfate) ion. The structure of the active-site cavity and conformational changes of the enzyme upon AZT binding are described in detail. It is found that the position of AZT differs remarkably from the positions of the pyrimidine bases and nucleoside analogues in other known complexes of pyrimidine phosphorylases, but coincides well with the position of 2′-fluoro-3′-azido-2′,3′-dideoxyuridine (N_3FddU) in the recently investigated complex of *E. coli* TP with this ligand (Timofeev *et al.*, 2013). The peculiarities of the arrangement of N_3FddU and 3′-azidothymidine in the nucleoside binding pocket of TP and correlations between the arrangement and inhibitory properties of these compounds are discussed.

1. Introduction

Thymidine phosphorylases (TPs; EC 2.4.2.4) are key enzymes in nucleoside metabolism. In the presence of inorganic phosphate, they catalyze the reversible phosphorolysis of the glycosidic bond in thymidine- and uridine-2′-deoxyribosides, with the formation of free base and deoxyribose 1-phosphate (Walter *et al.*, 1990; Bicknell & Harris, 1996). The reaction between nucleoside and phosphate ions bound to the enzyme in the nucleoside and phosphate binding pockets, respectively, proceeds by means of the nucleophilic attack of the phosphate O atom on the C1′ atom of the deoxyribose ring (Schwartz, 1971; Rick *et al.*, 1999).

In addition to phosphorolysis, thymidine phosphorylases catalyze the transfer of the deoxyribosyl moiety from one pyrimidine base to another. This transglycosylation reaction plays a key role in the salvage pathway of nucleoside biosyntheses, providing an alternative to the *de novo* purine

and pyrimidine biosynthetic pathways (Friedkin & Roberts, 1954; Leer *et al.*, 1977).

Mammalian thymidine phosphorylases stimulate tumour growth, and their level is enhanced in tumour cells, where they are involved in angiogenesis and development of metastasis (Bicknell & Harris, 1996; Matsushita *et al.*, 1999). Thus, TP is a suitable target in a search for anticancer and antiviral drugs. In addition, TP provides the activation of some anticancer prodrugs (Bronckaers *et al.*, 2009).

Owing to their ability to catalyze transglycosylation, some bacterial TPs are widely used in biotechnology for the large-scale production of natural 2′-deoxy-β-D-ribonucleosides and their analogues containing modifications in the carbohydrate and base fragments (Mikhailopulo & Miroshnikov, 2011). Among these nucleosides are many biologically important compounds with anticancer and antiviral activity (Desgranges *et al.*, 1983; Woodman *et al.*, 1980; Schwartz *et al.*, 1995). Therefore, the search for compounds which are able to regulate or inhibit TP activity as well as study of the interactions of these compounds with TP is of special interest. Knowledge at the atomic level of the interaction of such compounds with TP and other enzymes of nucleoside metabolism is required for the rational design of new drugs and the engineering of new forms of the enzymes with altered selectivity.

There are two families of nucleoside phosphorylases, which differ remarkably in the type of quaternary structure and in polypeptide chain folding. TP belongs to the family II nucleoside phosphorylases; family II comprises all pyrimidine phosphorylases (PyNPs) except for uridine phosphorylase (Pugmire & Ealick, 2002). All bacterial and mammalian pyrimidine phosphorylases of family II display a dimeric quaternary structure with subunits consisting of a small α domain separated by a large cleft from a larger α/β domain (Pugmire & Ealick, 2002). The biologically active form of these enzymes is a dimer. The degree of sequence homology between the pyrimidine phosphorylases of the second family exceeds 40% (Fig. 1).

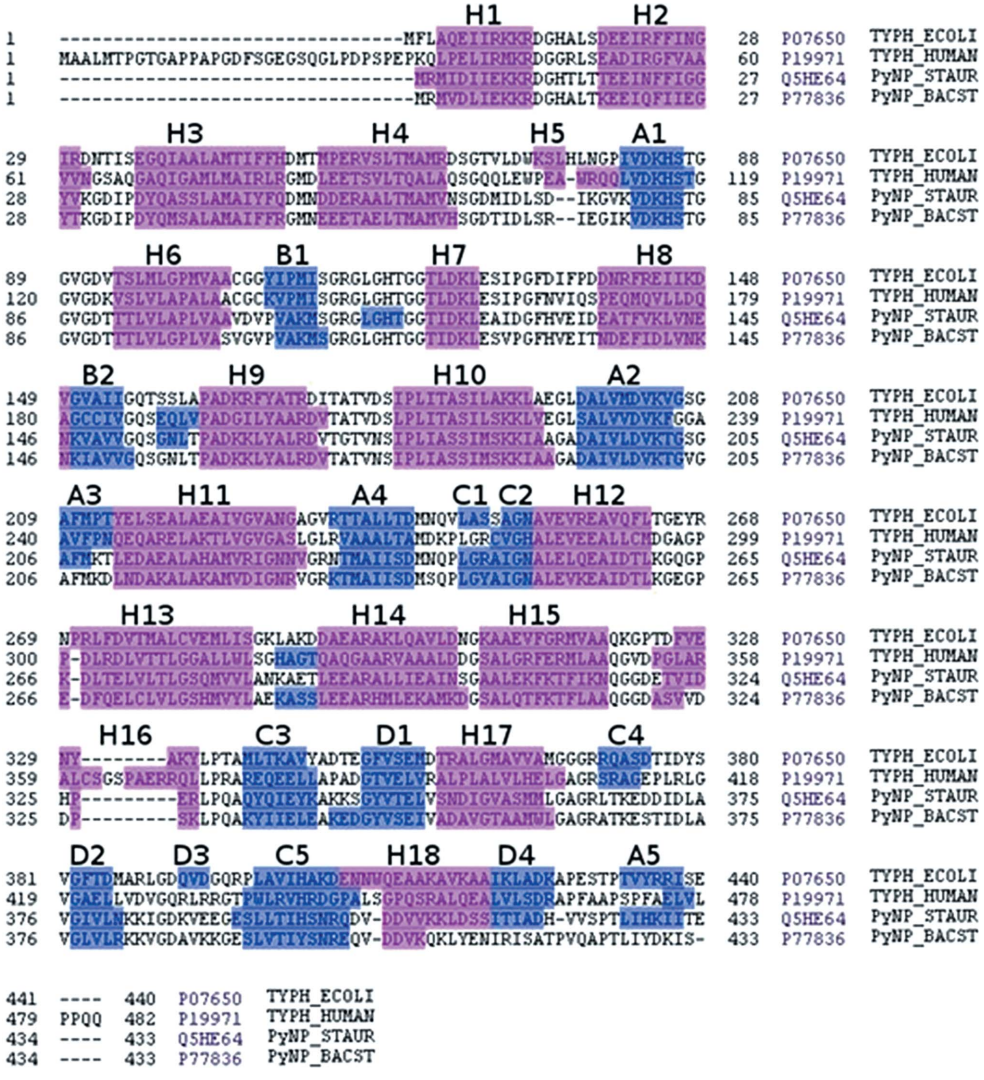

Figure 1
Alignment of the amino-acid sequences of several pyrimidine phosphorylases of family II: *E. coli* TP (TYPH_*E. coli*), human TP (TYPH_HUMAN), *S. aureus* PyNP (PyNP_STAUR) and *B. stearothermophilus* PyNP (PyNP_BACST); α-helices and β-strands are coloured magenta and blue, respectively. Helices are labelled H1–H18. Strands belonging to different sheets are labelled with the letters A, B, C and D.

The three-dimensional structures of some pyrimidine phosphorylases have been determined in the resolution range 1.5–3.0 Å both in the free state and in complex with inhibitors and nucleoside analogues. These include *Escherichia coli* TP (Walter *et al.*, 1990; Timofeev *et al.*, 2013), pyrimidine nucleoside phosphorylase from *Bacillus stearothermophilus* (BsPyNP) in complex with pseudouridine (Pugmire & Ealick, 1998), human TP in complex with inhibitor (Norman *et al.*, 2004) and with thymine (El Omari *et al.*, 2006), and PyNP from *Staphylococcus aureus* (PDB entry 3h5q; I. A. Shumilin, M. Zimmerman, M. Cymborowski, T. Skarina, O. Onopriyenko, W. F. Anderson, A. Savchenko & W. Minor, unpublished work). It has been shown that the active-site cavity of PyNP, which comprises phosphate and nucleoside binding pockets, is situated in the cleft between the large α/β domain and the small α domain. The subunits of the enzyme can be in either a closed (active) or an open (non-active) conformation (Pugmire *et al.*, 1998). As studied by a molecular-dynamics method,

Table 1
Kinetic parameters of thymidine phosphorolysis by thymidine phosphorylase at different concentrations of 3′-azido-3′-deoxythymidine.

AZT concentration (m*M*)	K_m (m*M*)	k_{cat} (s^{-1})	K_i (m*M*)
0	0.30 ± 0.03	217 ± 24	—
0.5	0.28 ± 0.07	108 ± 7	0.50 ± 0.07
0.8	0.28 ± 0.05	74 ± 7	0.41 ± 0.06
1.0	0.26 ± 0.04	89 ± 9	0.70 ± 0.12
7.0	0.20 ± 0.02	30 ± 1	1.12 ± 0.05

transition between the open and closed forms of the subunits is performed by means of domain movements, in which the domains move as rigid bodies (Pugmire & Ealick, 1998).

Recently, we have determined the X-ray structure of *E. coli* TP complexed with the reversible inhibitor 2′-fluoro-3′-azido-2′,3′-dideoxyuridine (N_3FddU) at 1.50 Å resolution; the structure of TP with sulfate (phosphate) only was refined at 1.55 Å resolution. The secondary structure of the enzyme is shown in Fig. 1 (Timofeev *et al.*, 2013). It has been found that N_3FddU, which contains fluorine and an azido group in the carbohydrate ring, binds to the enzyme in an unusual way. Its position only partly overlapped with the positions of other pyrimidine derivatives located in the nucleoside-binding pocket of pyrimidine phosphorylases, whereas the orientation of the pyrimidine rings and the arrangement of the carbohydrate fragments were remarkably different.

Here, we have studied the three-dimensional structure of *E. coli* TP complexed with 3′-azido-3′-deoxythymidine (AZT) at 1.52 Å resolution. This compound, which differs from thymidine, the natural substrate of TP, only by the N_3 group in the carbohydrate ring, is used widely for the treatment of viral infections, including human acquired immunodeficiency syndrome, owing to the ability of its phosphate derivatives to inhibit the viral reversible transcriptase (König *et al.*, 1989). Using kinetic measurements, we have shown that AZT is a reversible noncompetitive inhibitor of TP. It has also been found that position of AZT in the nucleoside binding site of *E coli* TP coincides almost completely with the position of N_3FddU in the TP–N_3FddU complex (Timofeev *et al.*, 2013) and they both differ from the position of the ligands located earlier in the nucleoside binding site (NBS). The possible role of the azido group as a trigger for the altered arrangement of AZT and N_3FddU is discussed, and the correlations between the positions of the ligands and their inhibitory activity are considered. An additional region of the active site is found to be involved in interaction with inhibitors. It is suggested that this phenomenon may be useful for the design of new TP inhibitors.

2. Materials and methods

2.1. Isolation and purification of recombinant TP

Recombinant TP was prepared in *E. coli* bacterial strain BL21(DE3)/pER_Thy1 and purified according to Esipov *et al.* (2002) and Kuranova *et al.* (2011).

2.2. Kinetic parameters for the phosphorolysis of thymidine by TP in the presence of AZT

Kinetic parameters for the phosphorolysis of thymidine by TP in the presence of AZT were measured in 50 m*M* potassium phosphate buffer pH 7 containing 0.06–1.8 m*M* thymidine, 0.36 mg ml^{-1} TP and different concentrations of AZT, as described in Timofeev *et al.* (2013). The kinetic parameters were determined by a nonlinear regression analysis using the *SciDAVis* software v.0.2.4. The inhibition constant for AZT was calculated according to the equation of non-competitive inhibition for each of the experiments on the basis of the observed maximum reaction rate at a given concentration of the inhibitor and the maximum rate in the absence of the inhibitor (Table 1). It was found that the maximum reaction rate decreases, while the Michaelis constant decreases slowly. Such a dependence is characteristic of partial noncompetitive inhibitors. The average K_i value is 0.68 ± 0.27 m*M*. These results are illustrated by Lineweaver–Burk plots (Fig. 2). Dilution of the reaction mixture increased the specific activity of the enzyme, which indicates that the inhibition is reversible.

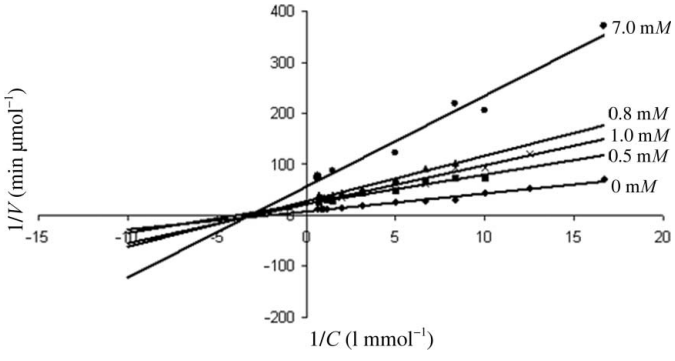

Figure 2
Lineweaver–Burk plot for thymidine phosphorolysis at various concentrations of azidothymidine.

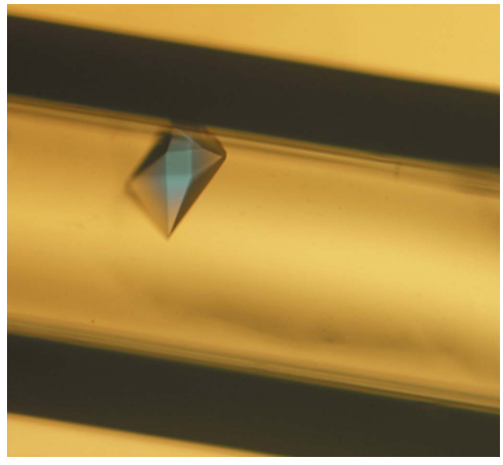

Figure 3
A crystal of *E. coli* thymidine phosphorylase grown in microgravity using the counter-diffusion technique.

Table 2
Statistical characteristics of the experimental data set and refinement of the structure of the TP–AZT complex.

Values in parentheses are for the highest resolution shell.

PDB code	4lhm
Data processing	
Space group	$P4_32_12$
Unit-cell parameters (Å, °)	$a = b = 130.7$, $c = 67.1$, $\alpha = \beta = \gamma = 90$
No. of molecules per asymmetric unit	1/2
Resolution (Å)	30.00–1.52 (1.56–1.52)
No. of unique reflections	89200
Multiplicity	9.2 (5.5)
Completeness (%)	99.8 (99.7)
$\langle I/\sigma(I)\rangle$	25.6 (2.1)
$R_{\rm mrgd\text{-}F}$ (%)	8.6 (52.9)
Refinement	
Resolution (Å)	1.52
No. of reflections used in refinement	83733
No. of reflections used in $R_{\rm free}$ calculation	4410
$R_{\rm cryst}/R_{\rm free}$ (%)	15.5/19.6
No. of refined non-H atoms in protein molecule	3387
No. of refined water molecules	485
No. of refined ATP atoms	19
No. of refined sulfate atoms	35
No. of refined glycerol atoms	12
B factors (Å^2)	
All atoms	30.1
Main chain	24.9
Side chains and protein-bound waters	34.5
R.m.s.d.	
Bond lengths (Å)	0.008
Angles (°)	1.250
Ramachandran plot†	
Most favourable areas (%)	94.0
Allowed areas (%)	6.0
Disallowed areas (%)	0

† The Ramachandran plot was created with the *PROCHECK* software (Laskowski *et al.*, 1993).

2.3. Crystallization of the TP–AZT complex

The crystals for X-ray study (Fig. 3) were grown in microgravity on the International Space Station by the counter-diffusion technique through a gel layer using ammonium sulfate as a precipitant (Kuranova *et al.*, 2011). Co-crystallization at a 20-fold excess of AZT was used for complex preparation. The protein solution consisted of TP at a concentration of 20 mg ml^{-1}, 0.02 *M* KH_2PO_4 pH 7.3, 0.04% NaN_3, 4 m*M* AZT. The composition of the precipitant solution was 30% ammonium sulfate in 0.05 *M* sodium citrate buffer pH 6.0, 4 m*M* AZT. The crystallization was carried out according to the protocol developed at JAXA, using the equipment provided by Confocal Science Co. as described previously (Takahashi *et al.*, 2010; Tanaka *et al.*, 2004).

2.4. X-ray data collection

X-ray data were collected from a single crystal of the TP–AZT complex at 100 K on beamline BL41XU at the SPring-8 synchrotron-radiation facility (Japan) equipped with an MX225HE CCD (MAR225HE) detector using the rotation method at a wavelength of 0.8 A. The rotation angle was 180°, the oscillation angle was 0.5° and the crystal-to-detector distance was 175 mm. Prior to flash-cooling, the crystals were soaked for a short time in a cryoprotectant solution. The cryoprotectant solution consisted of the precipitant solution with 20% glycerol and 10 m*M* AZT. The experimental intensities were processed to 1.52 Å resolution using the *HKL*-2000 program package (Otwinowski & Minor, 1997). All crystals belonged to space group $P4_32_12$ and contained one subunit of a dimeric TP molecule in the asymmetric unit. The data-processing statistics are given in Table 2.

2.5. Structure solution and refinement

The crystal structure was solved by the molecular-replacement method using *Phaser* (McCoy *et al.*, 2007) with the atomic coordinates of apo *E. coli* TP at 2.6 Å resolution (PDB entry 2tpt; Pugmire *et al.*, 1998) as a starting model. Structure refinement was carried out using *REFMAC*5 (Murshudov *et al.*, 2011). Manual rebuilding of the model was performed using the *Coot* interactive graphics program (Emsley *et al.*, 2010), and electron-density maps were calculated with $2|F_o| - |F_c|$ and $|F_o| - |F_c|$ coefficients; a number of water molecules, glycerol molecules and several sulfate (or phosphate) ions were located in difference electron-density maps. The positions of AZT in the nucleoside binding pocket and sulfate (phosphate) ion in the phosphate binding pocket were located in the difference electron-density maps calculated with $|F_o| - |F_c|$ coefficients and refined with full occupancy. An OMIT electron-density map calculated with $|F_o| - |F_c|$ coefficients at 2σ for AZT is presented in Fig. 4.

The atomic coordinates of the TP–AZT complex have been deposited in the Protein Data Bank as PDB entry 4lhm.

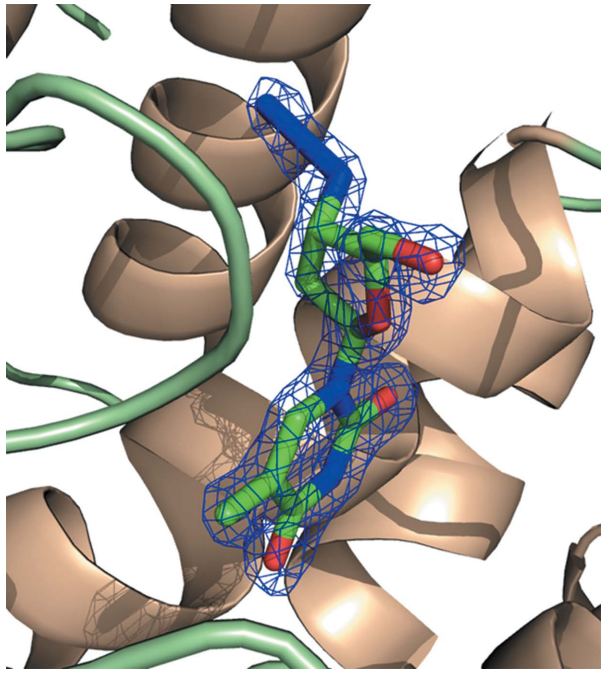

Figure 4
The molecule of 3′-azidothymidine in the nucleoside binding pocket of *E. coli* thymidine phosphorylase. The electron density is calculated with $|F_o| - |F_c|$ coefficients at the 2.0σ level. The ligand was excluded in the calculation of the electron-density map.

2.6. Quality of the crystals and quality of the model

The crystals of the TP–AZT complex grown in microgravity through the gel layer by the counter-diffusion technique reached dimensions of 0.3 mm (Fig. 3) as described in Kuranova *et al.* (2011). They were used for X-ray data collection at the SPring-8 synchrotron-radiation facility.

X-ray data collected from space-grown crystals allowed the determination of the structure of the TP–AZT complex at 1.52 Å resolution. The electron-density map calculated with $2|F_o| - |F_c|$ coefficients showed clear density for the backbone, the majority of the amino-acid side chains and a number of water molecules, which formed a hydrogen-bond network in the active-site cavity. Because the protein was dissolved in potassium phosphate buffer and ammonium sulfate was used as a precipitant, several sulfate (or phosphate) ions were located in the electron-density map; one of these ions occupies the phosphate binding pocket in the active-site cavity.

3. Results and discussion

Study of the three-dimensional structures of the enzymes of nucleoside metabolism complexed with nucleoside analogues is of special interest because there are many compounds with therapeutic potential among the nucleoside analogues. Taking into account the therapeutic application of these compounds, it is essential to know whether antitumor or antiviral drugs are able to interact not only with their target proteins but with other enzymes of nucleoside metabolism.

Recently, we have studied the interaction of 3′-azido-2′-fluoro-2′,3′-dideoxyuridine (N_3FddU) with *E. coli* TP using enzyme kinetics and X-ray structure determination. This compound contains an azido group and an F atom as substituents in the deoxyribose ring. It is known that the introduction of F atoms or azido groups into the carbohydrate ring remarkably affects the pharmacological properties of the compound. We have shown that N_3FddU acts as a reversible non-competitive inhibitor of *E. coli* TP and binds to the enzyme in a special manner which was not previously known.

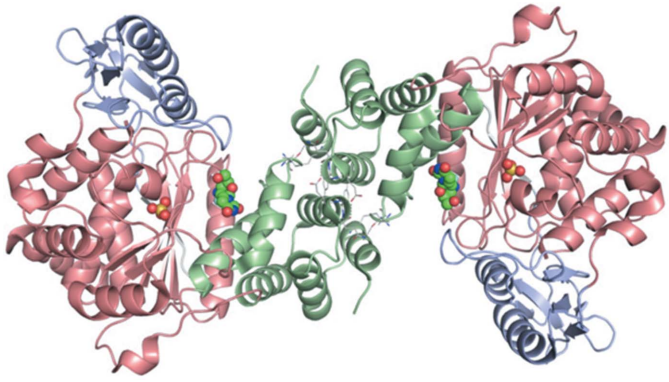

Figure 5
The dimeric molecule of *E. coli* thymidine phosphorylase with sulfate ion and 3′-azidothymidine bound in the active-site cavity. The atoms of the ligands are shown as spheres. Domains of subunits are coloured green (α domain), salmon (the N-terminal part of the α/β domain) and light blue (the C-terminal part of the α/β domain).

Here, the three-dimensional structure of *E. coli* thymidine phosphorylase has been determined in complex with the nucleoside antibiotic 3′-azido-3′-deoxythymidine (AZT). 3′-Azido-3′-deoxythymidine (or simply azidothymidine) is widely used for the treatment of human immunodeficiency virus (syndrome of acquired immunodeficiency; König *et al.*, 1989). AZT differs from thymidine, a natural substrate of thymidine phosphorylase, only by the replacement of the 3′-OH group with an azido group. AZT, as well as its C5′-monophosphate and triphosphate derivatives, interacts with reverse transcriptase and inhibits the binding of thymidylate (Ono *et al.*, 1986). There is sufficient evidence that AZT may be incorporated into viral DNA in place of thymidine and thereby terminate DNA chain elongation (St Clair *et al.*, 1985). It is possible to suggest that AZT, as a nucleoside analogue, is also able to interact with nucleoside phosphorylases; although it is not a substrate of TP. The results of a kinetic study showed that in the phosphorolysis reaction of thymidine catalyzed by *E. coli* TP, AZT acts as a reversible non-competitive inhibitor with an inhibition constant K_i of 0.68 m*M*.

According to X-ray study, the AZT molecule was located with full occupancy in the nucleoside binding pocket, whereas the phosphate binding pocket was occupied by sulfate (or phosphate) ion because the crystals of TP were grown with ammonium sulfate as precipitant and the protein was dissolved in 0.02 *M* KH_2PO_4. There is no possibility of distinguishing these ions in the electron-density map. We will refer to this ion as a sulfate in the following.

3.1. The overall structure of TP and the TP–AZT complex

The dimeric molecule of *E. coli* TP with sulfate ion in the phosphate binding pocket and AZT in the nucleoside binding pocket is shown in Fig. 5. The secondary structure is shown in Fig. 1. The overall structure of the TP molecule in the TP–AZT complex at 1.52 Å resolution is similar to the *E. coli* TP structure at 2.6 Å resolution (PDB entry 2tpt). Additionally, at higher resolution more water molecules are located, particularly in the functionally important areas. As will be described below, water molecules together with amino-acid residues and ligands participate in the formation of the general hydrogen-bond network in the active-site cleft.

As described previously by Walter *et al.* (1990), each subunit of the enzyme is composed of a small α-helical domain (residues 1–65 and 161–193), which consists of six α-helices H1–H4 and H9–H10, and a large α/β domain (residues 66–160 and 194–440). The α/β domain comprises 12 α-helices (H5–H8 and H11–H18) and four β-sheets; the strands of each β-sheet are labelled A, B, C and D (Fig. 1). The polypeptide chain topology presented according to the CATH classification attributes the region 337–433 near the C-terminal part of the α/β domain to a separate domain consisting of two α-helices (H17 and H18) and two β-sheets (C and D). The large flexible loop 367–381 between helix H17 and β-strand D2 limits the entrance to the active site. The protein polypeptide chain

crosses between the large and small domains three times (residues 66–71, 155–162 and 193–197).

The active site with nucleoside and phosphate binding pockets occupies the cleft between the large and small domains. The subunit interface is formed mostly by residues of the H3 helices of both subunits related by a twofold axis. There are also some residues of loop 173–178 in the interface which are situated near the bound nucleoside and connect helices H9 and H10 of the α domains.

3.2. The conformation of the subunits in the TP–AZT complex

As shown in Pugmire *et al.* (1998) and Pugmire & Ealick (1998), the subunits of pyrimidine phosphorylases can be in a closed (active) or an open (inactive) conformation. In the open conformation the substrates bound in the nucleoside and phosphate binding pockets are more distant from each other than in the closed conformation, and the active-site cavity is more accessible to solvent. In the closed conformation the substrates are brought closer to each other and the entrance to the active site is closed owing to the displacement of several flexible loops, in particular 367–381. The transition between the conformations proceeds by movement of the domains. The presence of the flexible loops allows the domains to move as rigid bodies relative to each other.

The superposition on C^{α} atoms of the TP–AZT complex and the open form of *E. coli* TP (PDB entry 1azy; Pugmire *et al.*, 1998) shows that the subunits in TP–AZT have an open conformation. This conclusion is confirmed by the superposition of the structures of TP–AZT and one of the subunits of *Bacillus stearothermophilus* PyNP (BsPyNP) complexed with uracil and phosphate ion (Pugmire & Ealick, 1998; PDB entry 1brw; Fig. 6). The latter is considered to be an example of the closed conformation. A significant difference between the two structures is observed in the positions of homologous flexible loops (loops 206–213, 173–178 and 367–381 in TP–AZT) which cover the entrance to the active-site cavity in the closed conformation. The shift between the C^{α} atoms of homologous phenylalanine residues, Phe210 in TP–AZT and Phe207 in BsPyNP, is 4.31 Å.

The shortest distance between the C^{α} atoms of Phe210 and Asp178 in the loop 173–181 in the TP–AZT complex is 9.42 Å, whereas the distance between the homologous residues Phe207 and Asp175 in BsPyNP is 5.14 Å. The distance between the C^{α} atoms of Ala373 of the flexible loop 367–381 and the C^{α} atom of Ile173 from the loop 173–179 located on the opposite side of the active-site cavity is 14.04 Å in TP–AZT, whereas the distance between the homologous residues in BsPyNP is 6.64 Å. Therefore, these data are consistent with the open conformation of the subunits in the TP–AZT complex.

The crystal packing of TP–AZT indicates that the open conformation of the subunits is

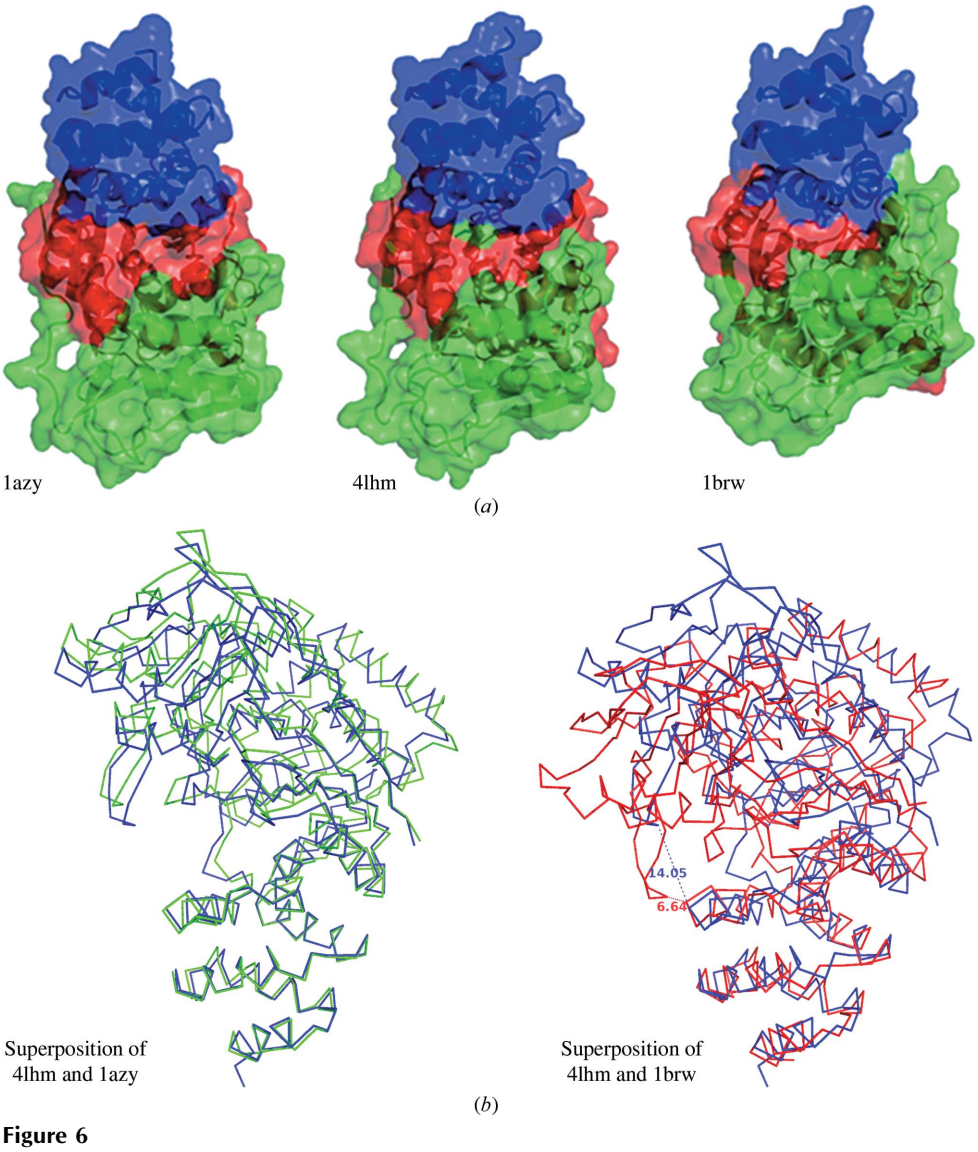

Figure 6
(*a*) The conformations of the subunits in *E. coli* TP (PDB entry 1azy), TP–AZT (PDB entry 4lhm) and *B. stearothermophilus* PyNP complexed with phosphate and uracil (PDB entry 1brw). The domains of the subunits are coloured dark blue (α-domain), red (the N-terminal part of the α/β domain) and green (the C-terminal part of the α/β domain). The subunits are shown in the same orientation. (*b*) The superposition on C^{α} atoms of *E. coli* TP–AZT subunit (blue) with the open form of *E. coli* apo TP (green, left) and with the closed form of BsPyN (red, right).

stabilized by intermolecular contacts in the crystal lattice. Several amino-acid residues of the flexible loop 367–381, which should move and cover the active-site cavity in the closed conformation, are involved in hydrogen bonds to amino-acid residues of a neighbouring molecule related by the symmetry operation $-y + 1/2$, $x - 1/2$, $z - 1/4$ (Fig. 7). For instance, the distances between the pair of atoms in two subunits, Gln372 OE1–Gln392′ N (3.02 Å), Ser374 O–Arg388′ NH2 (3.13 Å), Asp375 OD1–Arg397′ NH1 (3.08 Å), Asp375 OD1–Arg397′ NH2 (2.34 Å), Asp375 OD2–Arg397′ NH1 (3.11 Å), Thr376 OG1–Arg388′ NH2 (3.06 Å), Asp378 OD2–Glu266 OE2 (2.54 Å), Tyr379 N–Glu266′ O (2.91 Å) and Ser380 OG–Glu266′ OE2 (2.99 Å), do not exceed 3.13 Å (Fig. 7).

3.3. Phosphate and AZT in the active site of *E. coli* TP

The active-site cavity of *E. coli* TP with bound AZT and sulfate ion and the residues in the nearest vicinity of the ligands (≤4 Å) are shown in Fig. 8.

The ligands are located on opposite sides of the active-site cleft. The sulfate ion mimics phosphate, which acts as an attacking nucleophile in the catalyzed reaction (Pugmire & Ealick, 2002). It is coordinated predominantly by the residues of the large domain, whereas AZT is coordinated by the residues of the small α domain. The phosphate binding site is arranged between two strands near the C-terminal part of the central β-sheet of the α/β domain. Sulfate (phosphate) ion is accommodated near helices H5 and H6, β-strands A1 (82–86) and B1 (108–113) of the α/β domain and helix H10 (180–192) of the α domain. It is hydrogen-bonded directly to amino acids Ser86 (A1), Ser95 (H6), Ser113 (B1), Thr123 (H7) and Lys84 (A1), and to His85, Lys191 and Asp92 through water molecules. The majority of amino-acid residues around the sulfate ion belong to the α/β domain. The only exception is Lys191 from helix 10 of the α domain. In addition to those around the sulfate ion, there are ten molecules of water involved in the hydrogen-bond system of the active site (Fig. 8). It is worth noting that the environment of the nucleophilic centre is totally polar. The nearest amino-acid residues surrounding the phosphate (sulfate), such as His85, Ser95, Ser86, Ser113, Thr123, Lys84 and Lys191, are invariant in the pyrimidine nucleoside phosphorylases of family II. The participation of some of them (His85 and Tyr168) in enzyme activity has been confirmed by site-directed mutagenesis (Mitsiki *et al.*, 2009).

It has been suggested (Pugmire *et al.*, 1998) that positively charged Lys residues provide an orientation of the nucleophile appropriate for the reaction; His85 can regulate the nucleophilicity of the phosphate through the donation or acception of a proton in the consequent steps of the reaction, while serine and threonine residues can enhance the nucleophilic properties of the phosphate.

The nucleoside binding pocket is restricted by the amino-acid residues of helices H9 (Tyr168 and Arg171) and H10 (Ile183, Ser186 and Lys190), which are situated on the surface of the α domain facing the interdomain cleft, and by residues of helix H11 (Leu220) and β-strand A1 (His 85) of the α/β domain. There are some flexible loops which limit the interdomain cleft: 113–121, 206–212, 367–381 of the α/β domain and loop 173–179 of the α domain. Some of these loops, for instance the long flexible loop in the C-terminal domain 367–381 and the interdomain loop 155–160, provide access to the active site; loop 173–179 is included in the subunit interface.

Accommodated in this pocket, the AZT molecule interacts with amino-acid residues from both domains. The N3 atom of

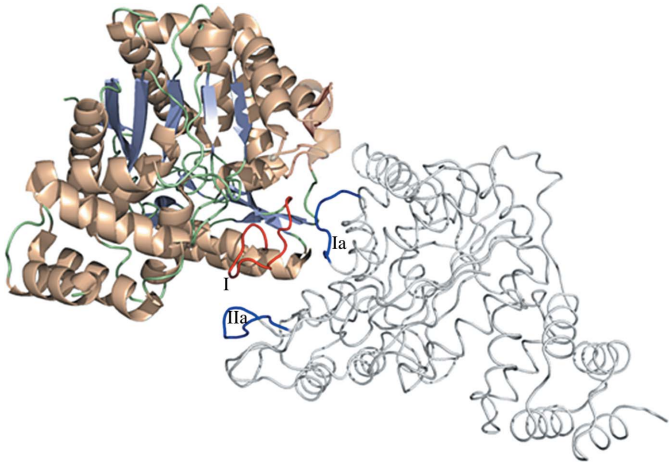

Figure 7
The intermolecular contacts in the crystal lattice of *E. coli* TP between the subunits of TP molecules related by the symmetry operation ($-y + 1/2$, $x - 1/2$, $z - 1/4$). The flexible loop which in the closed conformation covers the active site of one subunit, participating in the intermolecular contacts, is coloured red (I, residues 367–380). The regions of the neighbouring subunits participating in the intermolecular contacts are coloured blue (Ia, residues 264–270; IIa, residues 390–397).

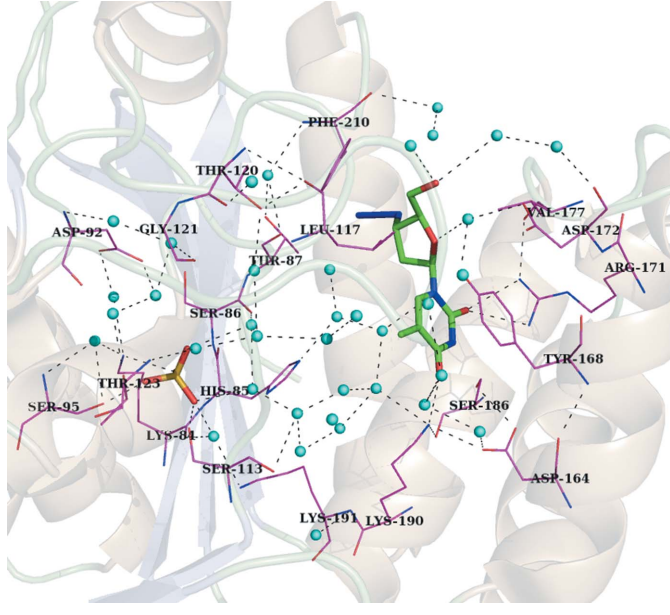

Figure 8
The nearest surroundings (≤4 Å) of 3′-azidothymidine and sulfate ion bound in the nucleoside and phosphate binding sites. Ligands are shown as sticks, water molecules are shown as blue spheres and hydrogen bonds are shown as dashed lines. The secondary structure is shown as a background.

the AZT pyrimidine ring forms a hydrogen bond to Ser186 O^{γ} (H10) of the α domain. The O2 and O4 atoms of the pyrimidine ring are hydrogen-bonded to the guanidine group of Arg171 (H9) and to Lys190 NZ (H10), respectively. It has been suggested that after cleavage of the glycosidic bond these amino acids stabilize the reaction transition state by proton donation to the pyrimidine base (Pugmire *et al.*, 1998). There is a stacking interaction between the pyrimidine ring of AZT and the aromatic ring of Tyr168 which is essential for enzyme activity. The replacement of this tyrosine by phenylalanine reduces the activity of thymidine phosphorylase, whereas its replacement by alanine eliminates activity completely (Mitsiki *et al.*, 2009). The 5-methyl group of the pyrimidine base is directed towards the cavity occupied by water molecules; the nearest residue to this group is Leu117.

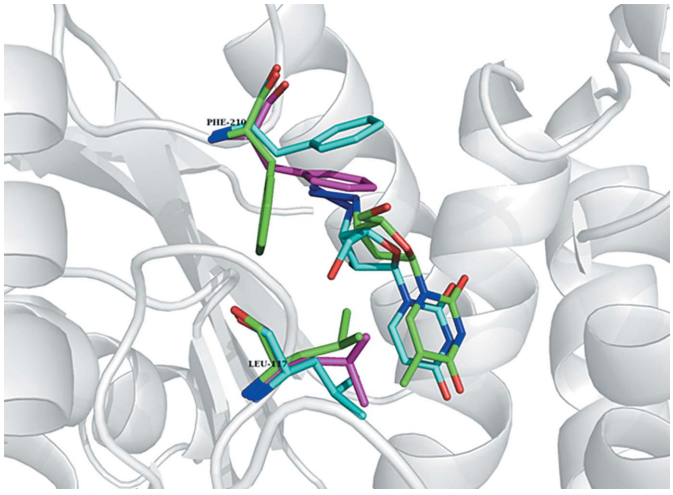

Figure 10
Conformational changes in thymidine phosphorylase upon binding AZT and N_3FddU. The structures of the free enzyme and the TP–AZT and TP–N_3FddU complexes are superimposed on C^{α} atoms. The side chains of free TP are coloured magenta, those of TP–AZT green and those of TP–N_3FddU blue.

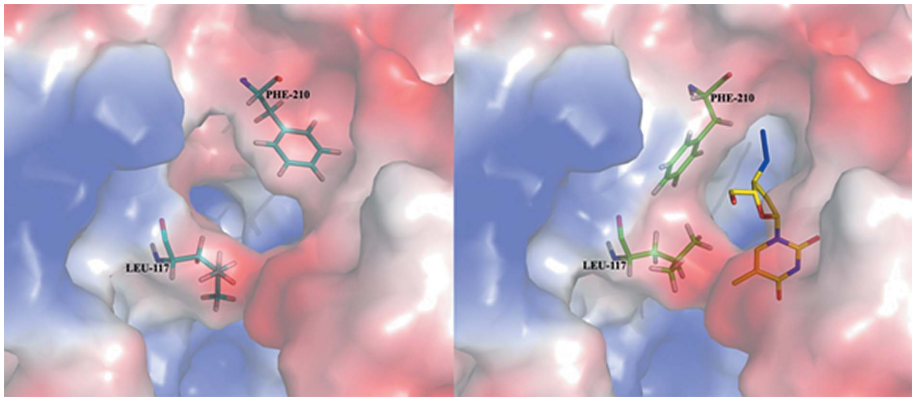

Figure 9
Formation of a hydrophobic pocket around the azido group in the nucleoside binding site of *E. coli* TP upon AZT binding. The surface of the enzyme is coloured according to the charge distribution. Left, the surface without ligand; right, the surface of the same region with bound AZT.

The deoxyribosyl ring of AZT is in close proximity to the α/β domain. The torsion angle of the glycosidic bond between the deoxyribose and pyrimidine rings which characterizes the mutual orientation of the deoxyribosyl and pyrimidine rings (O4′—C1′—N1—C2) is −136.15°, which corresponds to the *anti* conformation. The torsion angle C3′—C4′—C5′—O5′ characterizing the orientation of the O5′-hydroxylic group relative to the ribosyl ring is −174.79°.

The O5′ atom of AZT hydrogen bonds to Asp172 OD1 and Tyr168 OH *via* a water molecule. It is also close to Val177 $C^{\gamma 1}$ (loop 173–179). The loop 173–179 connecting helices H9 and H10 is part of the subunit interface.

The 3′-azido group is immersed into a hydrophobic pocket formed by amino-acid side chains of both domains: Leu220 (H11), Phe210 and Met211 (loop 204–214) of the α/β domain and Val177, Ile183 and Ile187 (helix H10 of the α domain). Most of these residues are invariant in pyrimidine nucleoside phosphorylases of family II. As will be shown below, this hydrophobic pocket is formed completely only after the binding of AZT (Fig. 8). The arrangement of the azido group in the hydrophobic pocket located between the large and small domains can prevent the movement of the domains and the proximity of the reaction centres. This finding explains the properties of AZT as a noncompetitive inhibitor.

3.4. The hydrogen-bond network in the active site of the TP–AZT complex

The remarkable peculiarity of the active-site cavity of TP is that more than 20 water molecules are located in this area (Fig. 8). This hydrogen-bond network through water molecules connects the amino-acid side chains with the bound ligands together and maintains the integrated active-site system. In the active site of TP, both ligands, AZT and sulfate ion, are arranged in different domains rather distant from each other. The distance between the nearest O atom of sulfate and the C1′ atom of the glycosidic bond which should undergo nucleophilic attack is 11.68 Å. Thus, a long distance between the ligands is typical for the open conformation of the subunits, which is also characterized by greater accessibility to the active-site cavity. However, even in the open conformation both of the ligands and the amino acids essential for activity are connected by numerous hydrogen bonds. For instance, His85 is hydrogen-bonded through one water molecule to the sulfate situated in the large domain and through two water molecules to the pyrimidine ring of AZT situated in the small domain.

The invariant lysine residues Lys190 and Lys191 also bind both ligands through hydrogen bonds. It is easy to suggest that the approach of the reaction centres during the transition to the closed conformation is accompanied by the displacement of water molecules from the active-site cavity. A similar

hydrogen-bond network has been found in the active site of TP complexed with N_3FddU (Timofeev *et al.*, 2013).

3.5. Conformational changes of TP upon AZT binding

Superposition on C^{α} atoms of the structures of TP with sulfate ion only and the TP–AZT complex reveals the conformational changes which accompany the binding of AZT (Fig. 9). The aromatic ring of Phe210 shifts towards the side chains of Thr87 and Leu117. This shift results in the formation of the hydrophobic pocket for accommodation of the 3′-azido group, comprising amino-acid residues from both domains: Ile183, Ile187, Leu220, Phe210 and Met211. In addition, the side chain of Leu117, which belongs to the flexible loop invariable in all pyrimidine phosphorylases, rotates and moves close to the C5′ atom of the deoxyribose ring and the C6 atom of the pyrimidine ring. Similar changes were observed upon binding of N_3FddU, the other nucleoside analogue containing an 3′-azido group. Superposition of the TP–AZT and TP–N_3FddU complexes reveals that both ligands with 3′-azido groups in the deoxyribose ring occupy nearly the same position. However, the conformations of the ligands are different. The torsion angle of the glycosidic bond O4′—C1′—N1—C2 in TP–AZT is −136.15°, whereas in TP–N_3FddU this angle is −111.73°. Also, upon N_3FddU binding the side chain of Phe210 moves in the opposite direction in comparison with AZT (Timofeev *et al.*, 2013). As a result, the 5′-hydroxymethylene groups of the deoxyribose are oriented differently; the distance between the C5′ atoms of the ligands in the superimposed complexes is 2.43 Å and the distances between the terminal N atoms of the azido groups is 1.16 Å (Fig. 10).

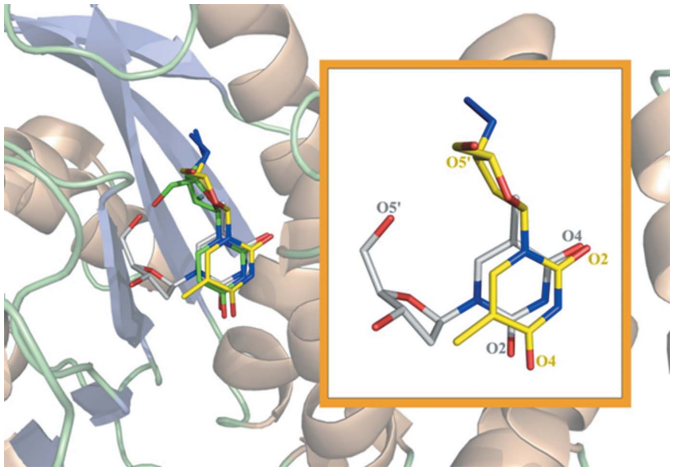

Figure 11
Comparison of the positions of AZT and N_3FddU in *E. coli* TP with the position of thymidine in *S. aureus* PyNP. The structures are superposed on three homologous residues bound to the pyrimidine ring. AZT is coloured yellow, N_3FddU green and thymidine grey. In the frame, the superposition of AZT and thymidine is shown separately.

3.6. Comparison of the arrangement of AZT in *E. coli* TP and the substrate thymidine in *S. aureus* pyrimidine nucleoside phosphorylase

The molecule of azidothymidine, which is a noncompetitive inhibitor of *E. coli* TP, differs from the natural substrate thymidine only by the azido group at the 3′-position of the deoxyribose ring. Therefore, comparison of the structure of *E. coli* TP–AZT with the structure of the homologous pyrimidine nucleoside phosphorylase (PyNP) from *S. aureus* complexed with thymidine (PDB entry 3h5q; Center for Structural Genomics of Infectious Diseases, unpublished work) allows elucidation of how the substitution at the 3′-position of the deoxyribose ring influences the arrangement of the ligands. The degree of homology between *E. coli* TP and *S. aureus* PyNP exceeds 40%. The comparison of the positions of thymidine and AZT in the corresponding complexes was performed by superposition of both structures on the C^{α} atoms of three homologous residues that are invariant in the family II pyrimidine phosphorylases (Fig. 11). These residues are Arg171, Ser186 and Lys190 in *E. coli* TP and Arg168, Ser183 and Lys187 in *S. aureus* TP. They all participate in the binding of pyrimidine bases in both enzymes.

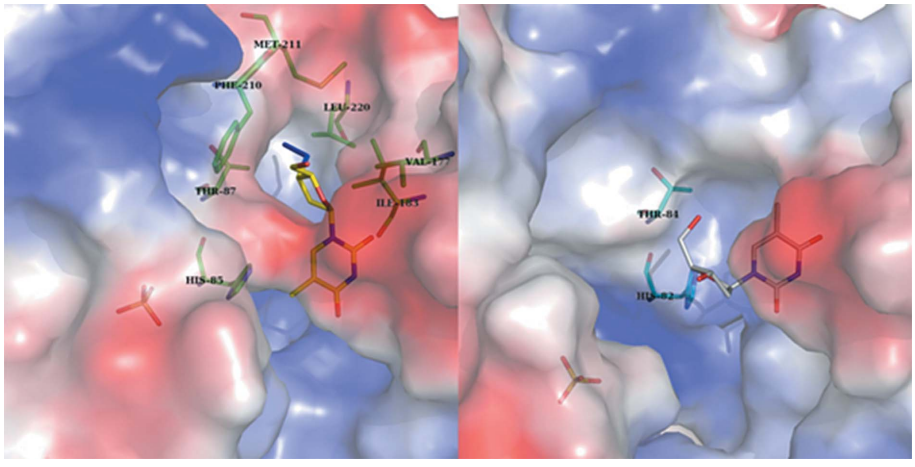

Figure 12
The surface of the nucleoside-binding pockets in *E. coli* TP with bound AZT (left) and in *S. aureus* TP with bound thymidine (right). The 3′-azido group of AZT directed into the hydrophobic pocket is coloured dark blue. The 3′-OH group of thymidine is coloured red. It is shown that the histidine residue essential for activity (His85 in *E. coli* TP) occupies different positions in both enzymes relative to the glycosidic bond. The structures are shown in the same orientation.

It was found that the positions of thymidine and AZT partly overlap. The planes of the pyrimidine rings of both ligands are superimposed almost completely (Fig. 11). However, the pyrimidine base in AZT–TP is rotated relative to the pyrimidine base of the thymidine in *S. aureus* PyNP by approximately 180° around the axis which crosses the N3 and C6 atoms of the pyrimidine rings. As a result, the amino-acid residues around the O2 and O4 atoms of the pyrimidine bases are different in the structures. The O2 atom of the pyrimidine ring in the AZT–TP

complex is hydrogen-bonded to the guanidine group of Arg171 and the O4 atom is hydrogen-bonded to the amino group of Lys190, whereas in the *S. aureus* PyNP–thymidine complex the O2 atom is hydrogen-bonded to Lys187 (Lys190 in *E. coli* TP) and the O4 atom is hydrogen-bonded to Arg168 (Arg171 in *E. coli* TP). It should be noted that in other known complexes of pyrimidine nucleoside phosphorylases with pyrimidine or nucleoside derivatives the orientation of the pyrimidine bases is the same as that of thymidine in the *S. aureus* PyNP–thymidine complex (PDB entries 1tpt and 1brw; Walter *et al.*, 1990; Pugmire & Ealick, 1998). Taking into account that the putative role of amino-acid residues bound to the O atoms of the pyrimidine ring is the stabilization of the transition state of the reaction, the described changes should not be crucial. However, the reorientation of the AZT pyrimidine base leads to a significant alteration in the surroundings of the deoxyribosyl moiety in TP–AZT in comparison with *S. aureus* PyNP–thymidine (Fig. 12). In the superimposed structures the distances between the C1′ atoms of the glycosidic bonds is 4.73 Å and the distances between the C4′ and C5′ atoms of the deoxyribose fragments are 5.72 and 4.77 Å, respectively. The 3′-OH groups and 3′-azido groups of the ligands are oppositely directed. The close vicinity of the 3′-OH group of the thymidine to Tyr165 OH is essential for enzyme activity (Tyr168 in *E. coli*), whereas the 3′-azido group of AZT is accommodated in the hydrophobic pocket formed by residues Ile183 and Ile187 (small domain) and Leu220, Phe210 and Met211 (large domain). The torsion angles of the glycosidic bond O4′—C1′—N1—C2 in both complexes corresponds to the *anti* conformation (−148.66° in *S. aureus* TP–thymidine and −136.19° in *E. coli* TP–AZT). The torsion angles C3′—C4′—C5′—O5′, which describe the orientation of the O5′ hydroxylic group relative to the ribose ring, differ remarkably: 50.31° in *S. aureus* TP–thymidine and −174.79 in *E. coli* TP–AZT. As a consequence, the positions of amino-acid residues essential for activity as well as the position of the attacking nucleophile (phosphate ion) relative to the glycosidic bond in the AZT–TP complex are unfavourable for the reaction to proceed. This finding explains the stability of the glycosidic bond in the TP–AZT as well as in the TP–N_3FddU complexes. On the other hand, the partial overlapping of the positions of AZT and thymidine explains the inhibitory action of AZT. The inhibitory action of AZT may also depend on the location of AZT between two domains so that the 3′-azido group is surrounded by residues from both domains. Owing to this, the AZT molecule can act as a spacer preventing movement of the domains and can hinder the formation of the active closed conformation.

As mentioned above, the positions of both compounds containing a 3′-azido group, AZT and N_3FddU, are very similar. It allows us to suggest the azido group to be the trigger of the reorientation of these ligands in the nucleoside binding pocket of TP. The phenomenon of reorientation as well as the formation of the hydrophobic pocket around the substituent in the 3′-position of the nucleoside can be used for the development of new types of selective inhibitors of thymidine phosphorylases.

This work was supported by the Central Scientific Research Institute of Machine-building of the Russian Federal Space Agency (Roscosmos) and RFBR grant 13-04-01100. We thank our Japanese colleagues K. Ohta, H. Tanaka, K. Inaka and their coworkers for helpful advice, loading and assembling the JCB crystallization box and for their assistance in collecting X-ray diffraction data sets at the SPring-8 synchrotron-radiation facility.

References

Bicknell, R. & Harris, A. L. (1996). *Curr. Opin. Oncol.* **8**, 60–65.
Bronckaers, A., Gago, F., Balzarini, J. & Liekens, S. (2009). *Med. Res. Rev.* **29**, 903–953.
Desgranges, C., Razaka, G., Rabaud, M., Bricaud, H., Balzarini, J. & De Clercq, E. (1983). *Biochem. Pharmacol.* **32**, 3583–3590.
El Omari, K., Bronckaers, A., Liekens, S., Pérez-Pérez, M. J., Balzarini, J. & Stammers, D. K. (2006). *Biochem. J.* **399**, 199–204.
Emsley, P., Lohkamp, B., Scott, W. G. & Cowtan, K. (2010). *Acta Cryst.* D**66**, 486–501.
Esipov, R. S., Gurevich, A. I., Chuvikovsky, D. V., Chupova, L. A., Muravyova, T. I. & Miroshnikov, A. I. (2002). *Protein Expr. Purif.* **24**, 56–60.
Friedkin, M. & Roberts, D. (1954). *J. Biol. Chem.* **207**, 245–256.
König, H., Behr, E., Löwer, J. & Kurth, R. (1989). *Antimicrob. Agents Chemother.* **33**, 2109–2114.
Kuranova, I. P., Smirnova, E. A., Abramchik, Y. A., Chupova, L. A., Esipov, R. S., Akparov, V. K., Timofeev, V. I. & Kovalchuk, M. V. (2011). *Crystallogr. Rep.* **56**, 884–891.
Laskowski, R. A., MacArthur, M. W., Moss, D. S. & Thornton, J. M. (1993). *J. Appl. Cryst.* **26**, 283–291.
Leer, J. C., Hammer-Jespersen, K. & Schwartz, M. (1977). *Eur. J. Biochem.* **75**, 217–224.
Matsushita, S., Nitanda, T., Furukawa, T., Sumizawa, T., Tani, A., Nishimoto, K., Akiba, S., Miyadera, K., Fukushima, M., Yamada, Y., Yoshida, H., Kanzaki, T. & Akiyama, S. (1999). *Cancer Res.* **59**, 1911–1916.
McCoy, A. J., Grosse-Kunstleve, R. W., Adams, P. D., Winn, M. D., Storoni, L. C. & Read, R. J. (2007). *J. Appl. Cryst.* **40**, 658–674.
Mikhailopulo, I. A. & Miroshnikov, A. I. (2011). *Mendeleev Commun.* **21**, 57–68.
Mitsiki, E., Papageorgiou, A. C., Iyer, S., Thiyagarajan, N., Prior, S. H., Sleep, D., Finnis, C. & Acharya, K. R. (2009). *Biochem. Biophys. Res. Commun.* **386**, 666–670.
Murshudov, G. N., Skubák, P., Lebedev, A. A., Pannu, N. S., Steiner, R. A., Nicholls, R. A., Winn, M. D., Long, F. & Vagin, A. A. (2011). *Acta Cryst.* D**67**, 355–367.
Norman, R. A., Barry, S. T., Bate, M., Breed, J., Colls, J. G., Ernill, R. J., Luke, R. W. A., Minshull, C. A., McAlister, M. S. B., McCall, E. J., McMiken, H. H. J., Paterson, D. S., Timms, D., Tucker, J. A. & Pauptit, R. A. (2004). *Structure*, **12**, 75–84.
Ono, K., Ogasawara, M., Iwata, Y., Nakane, H., Fujii, T., Sawai, K. & Saneyoshi, M. (1986). *Biochem. Biophys. Res. Commun.* **140**, 498–507.
Otwinowski, Z. & Minor, W. (1997). *Methods Enzymol.* **276**, 307–326.
Pugmire, M. J., Cook, W. J., Jasanoff, A., Walter, M. R. & Ealick, S. E. (1998). *J. Mol. Biol.* **281**, 285–299.
Pugmire, M. J. & Ealick, S. E. (1998). *Structure*, **6**, 1467–1469.
Pugmire, M. J. & Ealick, S. E. (2002). *Biochem. J.* **361**, 1–25.
Rick, S. W., Abashkin, Y. G., Hilderbrandt, R. L. & Burt, S. K. (1999). *Proteins*, **37**, 242–252.
Schwartz, E. L., Baptiste, N., Megati, S., Wadler, S. & Otter, B. A. (1995). *Cancer Res.* **55**, 3543–3550.
Schwartz, M. (1971). *Eur. J. Biochem.* **21**, 191–198.
St Clair, M. H., Weinhold, K., Richards, C. A., Barry, D. W. & Furman, P. A. (1985). *Program and Abstracts of the 25th Interscience*

Conference on Antimicrobial Agents and Chemotherapy, p. 439. Washington: American Society for Microbiology.
Takahashi, S., Tsurumura, T., Aritake, K., Furubayashi, N., Sato, M., Yamanaka, M., Hirota, E., Sano, S., Kobayashi, T., Tanaka, T., Inaka, K., Tanaka, H. & Urade, Y. (2010). *Acta Cryst.* F**66**, 846–850.
Tanaka, H., Inaka, K., Sugiyama, S., Takahashi, S., Sano, S., Sato, M. & Yoshitomi, S. (2004). *J. Synchrotron Rad.* **11**, 45–48.
Timofeev, V. I., Abramchik, Y. A., Fateev, I. V., Zhukhlistova, N. E., Murav'eva, T. I., Kuranova, I. P. & Esipov, R. S. (2013). *Crystallogr. Rep.* **58**, 842–853.
Walter, M. R., Cook, W. J., Cole, L. B., Short, S. A., Koszalka, G. W., Krenitsky, T. A. & Ealick, S. E. (1990). *J. Biol. Chem.* **265**, 14016–14022.
Woodman, P. W., Sarrif, A. M. & Heidelberger, C. (1980). *Cancer Res.* **40**, 507–511.